

ARTICLE

Received 15 Nov 2014 | Accepted 19 Jul 2015 | Published 18 Sep 2015

DOI: 10.1038/ncomms9104

OPEN

Dynamical backaction cooling with free electrons

A. Niguès¹, A. Siria¹ & P. Verlot²

The ability to cool single ions, atomic ensembles, and more recently macroscopic degrees of freedom down to the quantum ground state has generated considerable progress and perspectives in fundamental and technological science. These major advances have been essentially obtained by coupling mechanical motion to a resonant electromagnetic degree of freedom in what is generally known as laser cooling. Here, we experimentally demonstrate the first self-induced coherent cooling mechanism that is not mediated by an electromagnetic resonance. Using a focused electron beam, we report a 50-fold reduction of the motional temperature of a nanowire. Our result primarily relies on the sub-nanometre confinement of the electron beam and generalizes to any delayed and spatially confined interaction, with important consequences for near-field microscopy and fundamental nanoscale dissipation mechanisms.

¹Laboratoire de Physique Statistique de l'Ecole Normale Supérieure, UMR8550, ENS, 24, rue Lhomond, 75005 Paris, France. ²Institut Lumière Matière, UMR5306 Université Lyon 1-CNRS, Université de Lyon, 69622 Villeurbanne Cedex, France. Correspondence and requests for materials should be addressed to P.V. (email: pierre.verlot@univ-lyon1.fr).

Coherent manipulation of mechanical motion is one of the great challenges of Modern Physics¹: driven by such outstanding goals as reaching the zero-point motion fluctuations of single quantum objects^{2,3}, observing the quantum behaviour of large atomic ensembles^{4–6}, or engineering systems for quantum information processing⁷, a number of efficient schemes have been proposed and implemented^{8–11}, establishing laser control as a paradigm for cooling and trapping matter at the microscopic scale¹². In recent years, the field of cavity optomechanics has demonstrated that this paradigm extends remarkably well to the macroscopic level^{13,14}, with demonstrations of radiation-pressure-induced cooling^{15,16} down to the quantum ground state^{17,18}.

Despite a considerable variability both in concepts and experimental realizations, all the above cited experiments relied on the fundamental interactions between a mechanical degree of freedom and an electromagnetic resonance (for example, atomic transitions¹⁹, Fabry–Perot resonance²⁰, two-level systems^{21–23}) that collects the mechanical energy.

In this work, we report the first dynamical backaction cooling experiment that is not mediated by an electromagnetic resonance. We demonstrate that under the illumination of a continuous focused electron beam, a nanowire can spontaneously reach an equilibrium with drastically reduced motional temperature. We develop a simple and general model and attribute this behaviour to the presence of dissipative force gradients generated by the electron-nanowire interaction. From a general perspective, our results point out the potential of spatial confinement to provide the same functions as optical confinement in laser cooling, with important consequences for interpreting and controlling near-field dynamics at the nanoscale^{24–27}. Moreover, the dramatic spatial dependence of the effectively measured mechanical damping rate emphasizes the prominent importance of taking into account the spatial environment for explaining dissipation mechanisms at the nanoscale, whose fundamental limits remain an opened question^{28–32}. In a more specific scope, our work shows that electron microscopy is perfectly suited to ultra-sensitive, perturbation-free dynamical studies at the nanoscale, with performances comparable to laser sensing^{33,34}, however with a 100 times higher confinement. This represents a very attractive perspective for sensitive investigation of mono-dimensional structures dynamics such as carbon nanotubes³⁵ and graphene³⁶. Last, on a more technical side, our results show

that electron microscopy intrinsically holds the ability to suppress the unavoidable thermal vibrations of nano-structures, yielding to a significant improvement of the image resolution.

Results

Detecting nanoscale dynamics with a SEM. The nano object of interest in this work consists of a cylindrical Silicon Carbide (SiC) nanowire with length $L = 150 \mu\text{m}$ and diameter $d = 250 \text{ nm}$. The nanowire is glued at the edge of a Tungsten micro-tip sitting on an Aluminium sample holder. The ensemble is mounted in vacuum onto the (grounded) three-dimensional-positioning stage hosted in a commercial scanning electron microscope (SEM; NOVA NANOSEM, FEI), see Fig. 1a. Scanning electron microscopy provides an image of the surface of a given sample through its response to a focused beam of electrons. The collisions between the incident electrons and the sample yield to a variety of interaction products, including light, X-rays and electrons, which can be further detected and used for imaging purposes³⁷. In this study, we will focus our interest on the so-called secondary electrons (SEs), which are ejected from the sample owing to strongly inelastic collisions between the primary electron beam and the surface of the target. These electrons are guided to a dedicated detector (Everhart–Thornley Detector), which includes a strongly biased grid and a high bandwidth scintillator. Importantly, secondary emission is an absorption sensitive mechanism and therefore captures both relief and composition, making SE response the most used imaging mode in SEM.

Here we turn secondary emission from its conventional use and show that it intrinsically holds additional capabilities for sensitive dynamical studies³⁸. The idea is depicted in Fig. 1b: scanning an individual nano object in a given direction x , its presence is revealed under the form of a sharp peak. Its nanomechanical displacements δx around its rest position x_0 will therefore result in large variations of the SE emission rate $\delta I_{\text{SE}}(t) \simeq (\partial I_{\text{SE}}/\partial x)_{x_0} \times \delta x(t)$, with $I_{\text{SE}}(x)$ denoting the average SE emission rate as a function of position x . The efficiency of such a scheme is primarily determined by the SE response contrast, which is typically high for a wide class of nano-objects and materials³⁹.

We have used this principle for sensitive motion detection and characterization of the SiC nanowire introduced above. All the measurements presented hereafter have been obtained with an

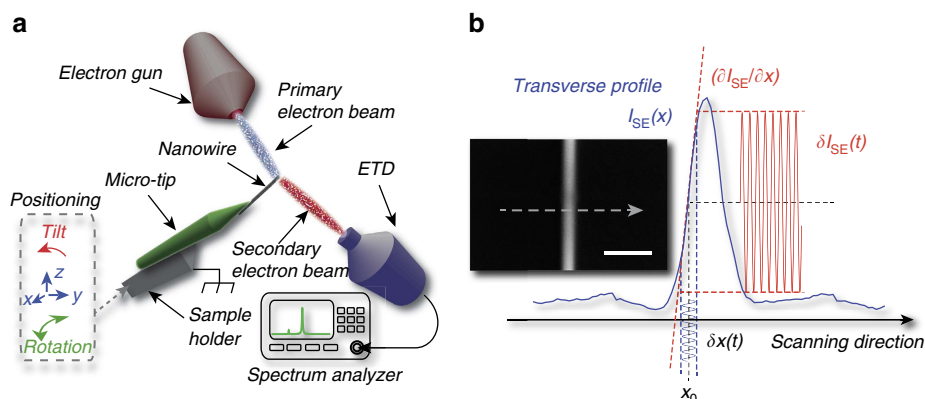


Figure 1 | Detecting nanoscale dynamics with a SEM. (a) Schematic of the experimental set-up. The nanowire is mounted onto the three-dimensional-positioning platform of a commercial SEM, which includes an electron gun delivering a stable collimated flux of electrons, and a SEs detector (Everhart–Thornley Detector (ETD)), whose output is used for both imaging the nanowire and measuring its dynamical motion around its equilibrium position.

(b) Using Secondary Emission for nanomechanical motion detection. The very high contrast of SEM imaging (illustrated here with a 20 nm gold nanowire, scale bar, 200 nm) results in a highly peaked evolution of the SE rate as a function of the transverse displacement. The nanomechanical motion δx around its equilibrium position x_0 is therefore transduced into large variation of the SE emission rate.

incident electron beam current $I^{\text{in}} = 140 \text{ pA}$ and an accelerating voltage $V = 5 \text{ kV}$, corresponding to an incident power $P^{\text{in}} = 0.7 \text{ } \mu\text{W}$. Figure 2a shows two SEM images (with magnification coefficients of $\times 1,500$ and $\times 250,000$, respectively). A very high contrast can be observed, suggesting a very efficient motional transduction into the SE emission rate. To further verify this assertion, we turn the SEM into ‘spot mode’ operation. We set the primary electron beam at position ($x_0 = -100 \text{ nm}$, $y_0 = 10 \text{ } \mu\text{m}$) (x and y denote the transverse and longitudinal coordinates with respective origins taken on the axis of the nanowire and at its clamping point, see Fig. 2a). The SE emission rate is collected via the real-time detector output of the SEM and further sent to a spectrum analyser. Two peaks are found around a frequency $\Omega/2\pi \approx 20 \text{ kHz}$ (see Fig. 2b), in agreement with the theoretically expected fundamental resonance frequency $\Omega_{0,\text{th}}/2\pi \approx 0.28/L^2 \sqrt{Ed^2/4\rho} \approx 18 \text{ kHz}$ (SiC density $\rho \approx 3,000 \text{ kgm}^{-3}$, and Young’s modulus $E \approx 400 \text{ GPa}$). We verified the presence of a pair of resonances around $\Omega/2\pi \approx 120 \text{ kHz}$ (Fig. 2c), corresponding to approximately six times the fundamental resonance frequency, and thereby completing the series of eigenmodes associated with a free-standing cantilever beam. We have also calibrated the measured spectrum into an equivalent transverse displacement (Fig. 2b). This is accomplished by dividing the measured fluctuations by the static transduction factor, that is, the slope $(\partial I_{\text{SE}}/\partial x)_{x_0, y_0}$ inferred from the line scan (inset, Fig. 2b). This calibration yields a displacement variance $\Delta x^2 = (68 \text{ pm})^2$. It is worth to compare this value to the thermal variance expected for such nanowire, $\Delta x_{\text{th}}^2 = k_B T / M_{\text{eff}}(y_0) \Omega_0^2$, with k_B Boltzmann’s constant, $T = 300 \text{ K}$ the ambient temperature, and $M_{\text{eff}}(y_0) = 0.23 M \frac{u^2(L)}{u^2(y_0)}$ the effective mass⁴⁰ (u being the mode shape function associated with the fundamental flexural mode of the nanowire and M the physical mass of the nanowire, $M = \rho \times \pi d^2 L/4$). For $y_0 = 10 \text{ } \mu\text{m}$, we find $\Delta x_{\text{th}}^2 = (50 \text{ pm})^2$, in very good agreement with the above calibrated value. We will henceforth assume the nanowire to be in contact with an external thermal bath with constant temperature $T = 300 \text{ K}$. Last, we have also measured spectra at various tilt angles (not shown), resulting in an effective rotation of the nanowire vibrational axis with respect to the horizontal plane. We have thus verified that the relative heights of both peaks seen in Fig. 2b could be changed and even inverted, which we have used to match both the scanning and vibrational planes. In the

following, we concentrate on the dynamical evolution of the in-plane vibration and will neglect the contribution of the out-of-plane mode to the measured nanomechanical spectrum.

Dynamics in retarded force gradients. The above reported thermal noise spectrum has been obtained within unfavourable measurement conditions, since the primary electron beam was coupled to the nanowire close to its anchor point, where its effective mass is very large (here $M_{\text{eff}}(y_0 = 10 \text{ } \mu\text{m}) = 130 \text{ ng}$). In a next step, we have therefore moved the electron probe towards the edge of the nanowire, expecting a rapid increase of the signal-to-noise ratio as a function of the longitudinal displacement y . Surprisingly, this is not what we observed: instead, the signal-to-noise ratio remained rather constant, whereas the spectral width of the transverse mode was dramatically increased (see Fig. 3b).

The displacements of the nanowire are governed by the general dynamical equation:

$$M_{\text{eff}}(L) \frac{\partial^2 x}{\partial t^2} = -kx(t) - M_{\text{eff}}(L) \Gamma_M \frac{\partial x}{\partial t} + F_{\text{th}}(t) + (R * F_{\text{ext}}(x_p))(t). \quad (1)$$

Here x denotes the transverse displacement of the nanowire, k its lateral spring constant, Γ_M its intrinsic damping rate, $F_{\text{th}}(t)$ the thermal Langevin force (with spectral density $S_F^{\text{th}}[\Omega] = 2M_{\text{eff}}(L)\Gamma_M k_B T$), F_{ext} the static external force field in which the nanowire is moving and x_p the time-dependent point of application of the force. The last term in equation (1) takes into account the external force changes Ω resulting from the nanomechanical motion³⁴, including some possible retardation effects through a time response $R(t)$. Keeping only the time-varying component of the displacements δx and δx_p and assuming that they remain small compared with the spatial variations of the external force, it is straightforward to expand equation (1) in Fourier space to obtain:

$$\chi^{-1}[\Omega] \delta x[\Omega] = F_{\text{th}}[\Omega] + R[\Omega] \frac{\partial F_{\text{ext}}}{\partial x} \Big|_{x_{p,\text{eq}}} \delta x_p[\Omega], \quad (2)$$

where Ω is the Fourier frequency, $\chi[\Omega] = 1/M_{\text{eff}}(L) (\Omega_0^2 - \Omega^2 - i\Gamma_M \Omega)$ is the mechanical susceptibility associated with the fundamental transverse vibration and $x_{p,\text{eq}}$ the static displacement of the nanowire at the point of application. In our

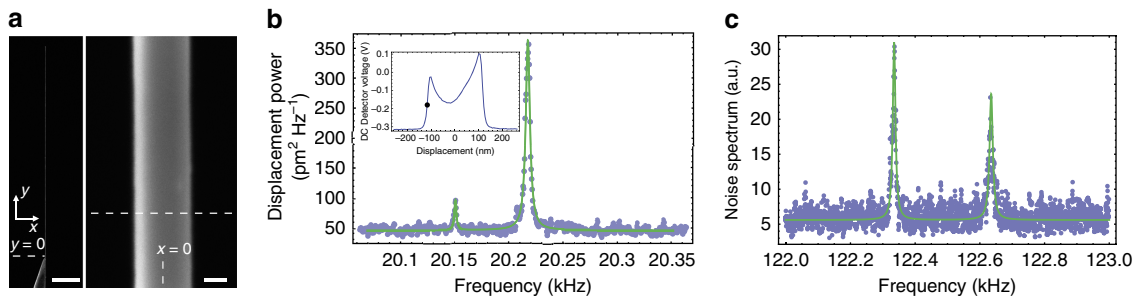


Figure 2 | Brownian motion detection of a SiC nanowire in a SEM. (a) SEM static images of the nanowire used in the present study. The magnification coefficients are $\times 1,500$ (left, scale bar, $20 \text{ } \mu\text{m}$) and $\times 250,000$ (right, scale bar, 100 nm). The nanowire is mounted into the horizontal plane (x, y), with respective origins on the nanowire axis (right) and at the apex of the Tungsten micro-tip (left). (b) Calibrated ETD noise spectrum $S_x[\Omega] = S_{I_{\text{SE}}}[\Omega]/G^2$ acquired in spot mode, with the electron probe being set at $y_0 = 10 \text{ } \mu\text{m}$. Inset shows a line scan taken at the same longitudinal distance, and which served for determining the local slope $G = (\partial I_{\text{SE}}/\partial x)_{x_{p,\text{eq}}, y_0}$. The dark dot indicates the transverse position at which the spectrum was acquired. (c) Brownian motion spectrum associated with the second harmonic vibration around $\Omega/2\pi \approx 122.5 \text{ kHz}$.

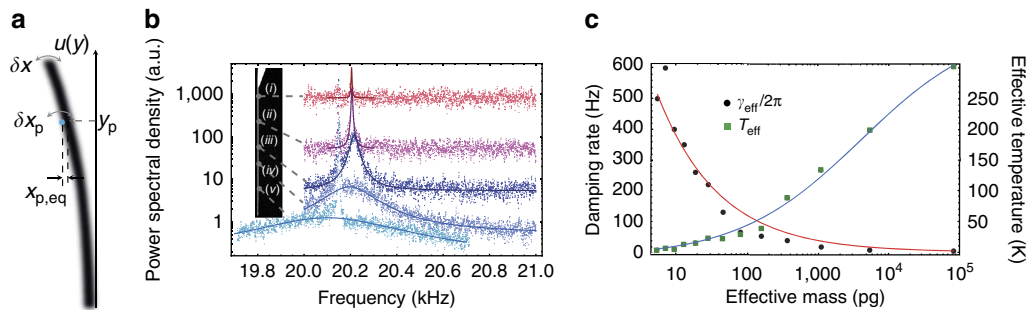


Figure 3 | Dynamical backaction cooling with electrons. (a) Schematic introducing the notations used in the text. The electron probe (blue spot) is at the average position $(x_{p,eq}, y_p)$. The dynamical displacement δx_p around the position of the probe and the tip displacement δx are related via the mode shape function u of the nanowire. (b) Dynamical backaction cooling using an electron beam. The longitudinal position of the electron spot is scanned across the entire nanowire length (left), with the transverse coordinate $x_{p,eq}$ being fixed. For each point, the corresponding fluctuation spectrum is recorded (acquisition time $\simeq 2$ min). The presented data are normalized to the same effective mass, to better visualize the drastic decrease of the effective temperature. Straight lines are a double Lorentzian adjustment of the experimental data. We attribute the observed amplification of the out-of-plane mode (left most peak) to the presence of orthogonal gradients. (c) Effective temperature (green squares) and effective damping rate (black dots) as functions of the effective mass. The straight lines correspond to plots of our theoretical model (equation 4), yielding $\Gamma_e(x_{p,eq})/2\pi = 604$ Hz.

case, the dominant external force being applied to the nanowire is generated by the primary electron beam, with point of application $(x_{p,eq}, y_p)$ (see notations in Fig. 3a). The displacement at the point of application are related to the displacement δx through the mode shape function u , $\delta x_p = \frac{u(y_p)}{u(L)} \delta x$, such that the equation of motion writes in Fourier space $\delta x[\Omega] = \chi_{eff}[\Omega] F_{th}[\Omega]$, with χ_{eff} given by:

$$\chi_{eff}^{-1}[\Omega] = \chi^{-1}[\Omega] - \frac{u(y_p)}{u(L)} R[\Omega] \left. \frac{\partial F_{ext}}{\partial x} \right|_{x_{p,eq}}. \quad (3)$$

Assuming that the spectral variations of R are negligible around frequency Ω_0 , equation (3) shows that our system is indeed expected to respond similarly to cavity optomechanical systems¹³, whose effective mechanical response is changed in presence of cavity-delayed optical force gradients. Such delays result in an additional imaginary contribution to the effective susceptibility (the cold damping term⁴¹, that would be equivalent to the imaginary part of R), which manifests as a change of the effective damping rate, and yields to the ability to control the dynamical state of the mechanical resonator.

As already noted above, we observe a very large increase of the effective dissipation when moving the probe towards the extremity of the nanowire, as shown in Fig. 3b. This suggests that important delays are involved into the dynamical interaction between the primary electron beam and the nanomechanical oscillator. This led us to identify the nature of this interaction as being of a thermal origin⁴²: when the electron beam hits the sample, a fraction of its energy is released into heat, as a consequence of inelastic mechanisms. To excite the acoustic phonon associated with the fundamental transverse vibrational mode, the produced heat needs to propagate over the entire length^{26,43}. Here we have assumed a first order low-pass model $R(t) = \frac{\Theta(t)}{\tau_{th}} e^{-\frac{t}{\tau_{th}}}$, with Θ the Heaviside step function, $\tau_{th} = L^2 \rho c_p / \kappa$ the heat diffusion time (c_p the specific heat capacity and κ the thermal conductivity). For SiC nanowires, typical values are on the order of $c_p \simeq 750 \text{ J K}^{-1} \text{ kg}^{-1}$ and $\kappa \simeq 10 \text{ W K}^{-1} \text{ m}^{-1}$, the latter being a factor of 10 lower than the bulk value, typically⁴⁴. Hence, we have for the product $\Omega_0 \tau_{th} \simeq 640 \gg 1$, which places our system into a situation equivalent to the resolved sideband regime for the electro-thermal backaction^{15,45}. This means that we can

retain the dissipative contribution of the backaction force only, and write the last term of equation (3) as purely imaginary, $i(u(y_p)/u(y_L)) \times M_{eff}(L) \Omega \Gamma_e(x_{p,eq})$. Finally, our theoretical analysis predicts the evolution of the effective mechanical damping rate Γ_{eff} and temperature $T_{eff} = \frac{M_{eff}(L) \Omega_0^2 (\Delta x)^2}{k_B}$ as a function of the probe longitudinal position:

$$\begin{aligned} \Gamma_{eff}(y_p) &= \Gamma_M + \frac{u(y_p)}{u(y_L)} \Gamma_e(x_{p,eq}), \\ T_{eff}(y_p) &= \frac{\Gamma_M}{\Gamma_{eff}(y_p)} \times T. \end{aligned} \quad (4)$$

Note that in equation (4), Γ_e , which represents the maximum dissipative coupling strength (when the probe hits the edge of the nanowire), has been assumed to only vary with the transverse degree of freedom x_p (and not y_p). This is justified because of the very homogeneous SE response of the nanowire (see Fig. 2a), which implies that the electron absorption rate (and hence the resulting thermal force) weakly depends on the longitudinal coordinate. In the low effective damping limit ($\Gamma_{eff} \ll \Omega_0$) and assuming a long heat diffusion time ($\Omega_0 \tau_{th} \gg 1$), it can be shown that $\Gamma_e(x_{p,eq}) = \frac{1}{\tau_{th}} \times \frac{1}{k} \left(\frac{\partial F_{ext}}{\partial x} \right)_{x_{p,eq}}$. We also emphasize the peculiar longitudinal dependence of the effective damping $u(y_p)/u(y_L) = \sqrt{M_{eff}(L)/M_{eff}(y_p)}$, proportional to the inverse square root of the effective mass. This is a signature of the local character of the dynamical backaction, which produces its ponderomotive effects exactly at the point of application, as demonstrated here for the first time.

Dynamical backaction cooling with a focused electron beam.

Figure 3b shows the spectral evolution of the transverse fundamental vibration when moving the probe from the anchor to the edge of the nanowire. The whole set of data were acquired for a value of $x_{p,eq} = -100$ nm. The spectra were normalized to the same effective mass, to better represent the dramatic reduction of the effective temperature (proportional to the spectrum area). One can also remark a slight shift of the mechanical resonance frequency at very high gains, characteristic of a residual in-phase contribution (similar to the ‘optical spring’) in the dynamical backaction. The experimental data are fitted to a Lorentzian

model. The fitting parameters enable to quantitatively determine the longitudinal evolution of both the effective damping rate $\Gamma_{\text{eff}}(y_p)$ and effective temperature $T_{\text{eff}}(y_p)$, shown in Fig. 3c (black dots and green squares, respectively). Here we chose to report their evolution as functions of the effective mass at the probe location $M_{\text{eff}}(y_p)$, which is a physically more representative parameter. The obtained results are in very good agreement with our theoretical description, as shown by the fitting curves (straight lines, derived from equation (4), with $\Gamma_M/2\pi = 4$ Hz and $T = 300$ K inferred from the reference thermal measurement shown in Fig. 2b) that adjust very well to our experimental data.

To further complete our study, we have also investigated the dynamical backaction effects when moving the equilibrium position of the probe in the transverse direction, for a fixed longitudinal coordinate $y_p = 40$ μm . The corresponding line scan is shown in Fig. 4a (dashed line). As already noted above, SE response reflects the primary electrons absorption rate, which is itself proportional to the force exerted by the electron beam. As a consequence, the strength of the dynamical backaction is expected to be proportional to the gradient of the SE emission rate, $(\partial F_{\text{ext}}/\partial x) \propto (\partial I_{\text{SE}}/\partial x)$. Figure 4a shows the theoretically expected backaction rate (straight, red line), obtained by normalizing the line scan derivative to the maximum backaction rate $\Gamma_{\text{ba}}(y_p) = \frac{u(y_p)}{u(L)} \Gamma_e(x_{p,\text{eq}} = -100 \text{ nm})$ inferred from the measurement presented in Fig. 3c. The right panel of Fig. 4 shows the results obtained at four illustrative transverse positions $x_{p,\text{eq}}$, labelled from (b–e). The resulting spectra show several interesting features that confirm our theoretical interpretation. Figure 4b,d are both obtained on regions of positive gradient, and are showing motion sensitivities and cooling rates that are proportional to the local slope, in very good agreement with the theoretically expected backaction rates. Figure 4c is obtained with the probe being set on a gradient-free spot, resulting in the total absence of electro-mechanical transduction. Finally, Fig. 4e corresponds to a negative slope, which conversely induces an important amplification of the Brownian motion (beyond the instability threshold, where the dynamical backaction rate cancels the intrinsic damping Γ_M). Importantly, the reversed behaviours observed in Fig. 4b,e reveal the asymmetry of the backaction force

with respect to the axis of the nanowire (see the cooling and heating domains in Fig. 4a). This asymmetry reflects that of the force exerted by the electron beam and is a signature of thermally induced bending at the nanoscale^{46,47}.

Discussion

Importantly, the ability to cool the motion fluctuations crucially relies on the ultra-low level of fluctuations associated with the cooling pump⁴¹. For the electron beam, these noises result from the electron shot noise $\delta I^{\text{in}}(t)$, characterized by the white spectral density $S_I^{\text{in}}[\Omega] = 2eI^{\text{in}}$ (e the positron charge). These fluctuations generate force noises that eventually limit the cooling efficiency^{45,48–50}. In general, the force noise associated with any given electron beam-mediated interaction F_k can be written $S_F^k[\Omega] = \Phi_k^2[V, \Omega] \frac{S_I^{\text{in}}[\Omega]}{e^2}$, with $\Phi_k[V, \Omega]$ denoting the interaction strength per electron per second. Our study gives a quantitative access to this latter quantity in the case of the electro-thermal interaction: From the above given expression of Γ_e , it is straight to obtain $\Phi_{\text{et}}[V, \Omega] \simeq \frac{\Gamma_e}{\Omega} \times \frac{k\Delta x_r}{(I^{\text{in}}/e)}$ (Δx_r the typical electro-thermal gradient range), where the $1/\Omega$ dependence results from high-frequency filtering of electro-thermal fluctuations. Taking $\Delta x_r = 10$ nm, $k = 7.9 \times 10^{-5} \text{ Nm}^{-1}$, and $\Gamma_e/2\pi = 604$ Hz (as extracted from the fits of the data shown in Fig. 3c), we find $\Phi_{\text{et}}[V, \Omega] \simeq 2.7 \times 10^{-23} \text{ N}(e^-)^{-1} \text{ s}^{-1}$, and an associated force noise $S_F^{\text{et}}[\Omega] \simeq (1.1 \text{ aN Hz}^{-\frac{1}{2}})^2$. On the other hand, the thermal noise evaluates on the order of $S_F^{\text{th}}[\Omega] = 2M_{\text{eff}}(L)\Gamma_M k_B T \simeq (31 \text{ aN Hz}^{-\frac{1}{2}})^2$: the force noise associated with the electro-thermal backaction is negligible compared with the thermal noise, which defines a cold damping mechanism and justifies that we have neglected it in equation (1).

It is also worth to consider the force noise associated with the ‘electronic pressure’ force, resulting from the momentum exchange between the incident electrons and the nanomechanical device. The corresponding interaction strength per electron per second identifies to the average lateral momentum loss per incident electron, $\Phi_p[V, \Omega] = \delta p_{\parallel}(V)$. Accurate evaluation of δp_{\parallel} is a complex problem a priori, requiring advanced simulations of electron transport inside the nanomechanical device⁵¹. Here we

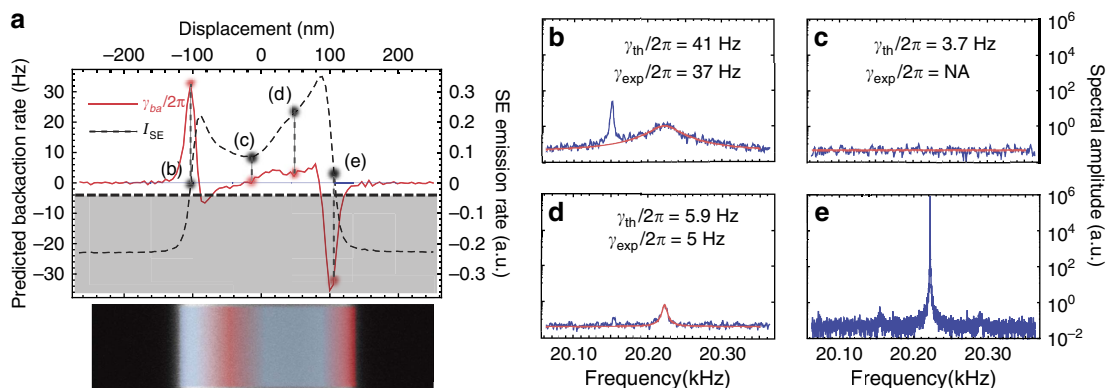


Figure 4 | Transverse evolution of the e-beam backaction. (a) Line scans of the SE emission rate (dashed, black line) and theoretically expected backaction rate $\Gamma_{\text{ba}} = \Gamma_{\text{eff}}\Gamma_M$ (straight, red line) obtained at the longitudinal position $y_p = 40$ μm . The grey zone represents the parametric instability region¹³, where the dynamical backaction cancels the intrinsic mechanical damping rate. Dots with abscissa (b–e) emphasize the values taken by I_{SE} and Γ_{ba} at the four acquisition spots. Heating and cooling regions are represented in red and blue on the SEM slice. Right panel: the SE emission rate fluctuation spectrum is measured at transverse positions $x_{p,\text{eq}}$ (b–e). The straight lines are Lorentzian adjustments to the experimental data.

derive a rough estimate by assuming that the single-electron incident lateral momentum noise $\delta p_{\parallel}(V) = \frac{\hbar}{\sqrt{2}w_0}$ is integrally transferred to the nanowire ($w_0 \simeq 1$ nm the waist of the electron beam), yielding to $\Phi_p[V, \Omega] \lesssim 7 \times 10^{-26} \text{ N}(\text{e}^-)^{-1} \text{ s}^{-1}$, and $S_F^p[\Omega] \lesssim (3 \times 10^{-21} \text{ N Hz}^{-\frac{1}{2}})^2$. Therefore, the ‘electronic pressure’ noise is negligible, the measurement being largely dominated by the quantum electro-thermal noise. This enables to subsequently quantify the quality of the measurement through evaluating the uncertainty products $\sqrt{S_x^r[\Omega] S_F^p[\Omega]} \simeq 1.6 \times 10^5 \frac{\hbar}{2}$ (ref. 22), where we have taken $S_x^r[\Omega] \simeq (7 \times 10^{-12} \text{ m Hz}^{-\frac{1}{2}})^2$ the measurement imprecision inferred from Fig. 2b. Therefore, our measurement scheme operates far above the Heisenberg limit, which is somehow not so surprising, since the measurement and backaction noises are referring to two electronic fields of distinct nature (that is, primary and secondary, respectively). Nevertheless, we note that significant improvement of this limit may be expected by measuring nanomechanical motion via the transmitted electron fluctuations, using for example, a scanning transmission electron microscopy detector.

Interestingly, the efficiency of electron beam cooling scales favourably at higher mechanical resonance frequency. Indeed, the backaction strength can be expressed as a function of the aspect ratio of the nanowire $a = L/d$, $\Gamma_e \simeq \frac{1}{\tau_{\text{th}}} \times \frac{x_s}{\Delta x_s} \propto a/d^2$, with $x_s = \tilde{\alpha}(L^2/d)\Delta T$ the static nanomechanical displacement⁴⁶ $\tilde{\alpha}$ the coefficient of thermal expansion, $\Delta T = \beta_{\text{abs}} R_{\text{th}} P^{\text{in}}$ the temperature elevation inside the nanowire, β_{abs} its energy absorption coefficient⁵² and $R_{\text{th}} = 4L/\pi d^2 \kappa$ its thermal resistance. Concurrently, the mechanical resonance frequency scales as $\Omega_0 \propto 1/a^2 d$: decreasing the diameter d while keeping the same aspect ratio therefore yields to both higher frequency and dynamical backaction effects. This perspective is particularly interesting in the context of coherent manipulation of ultra-low phonon number states, since the initial phonon occupancy scales as the inverse of the mechanical resonance frequency $n_0 = k_B T / \hbar \Omega_0$. Hence, our scheme may provide backaction rates as high as $\Gamma_e / 2\pi \simeq 2$ MHz for 1- μm long, high aspect ratio nano-structures ($a \gtrsim 100$), opening the perspective to cool these objects down to their quantum ground state⁵³.

In conclusion, we have shown that free electrons establish as an ultra-sensitive, non-invasive probe for measuring and manipulating nanomechanical motion at room temperature. Using a commercial SEM, we have demonstrated that beyond its exquisite static resolution, in the nm range, electron microscopy enables ultra-high, sub-atomic (5 pm range) dynamical sensitivity. We have shown that the SEM appears as an active device that can be used for manipulating the dynamics of a pg-scale nanomechanical device, via an ubiquitous electro-thermal mechanism that creates strong force gradients in the object, while weakly perturbing its static thermodynamic state. In particular, we have used this effect and reported a 50-fold suppression of the transverse vibrational mode thermal energy, representing the first self-induced cooling mechanism that is not mediated by an electromagnetic resonance, but entirely relies on the local force field spatial confinement. Our result therefore appears as a novel, quantitative tool for ultra-sensitive study of electron matter interaction phenomena at nanoscale.

Methods

Determination of the effective temperature. For each value of the longitudinal coordinate y_p , the spectrum of the SE emission rate fluctuations $S_{\text{SE}}[\Omega, y_p]$ is recorded together with the local slope $(\partial I_{\text{SE}}/\partial x)_{x_p, \text{eq}, y_p}$, with the transverse coordinate $x_p, \text{eq} = -100$ nm being fixed. Note that as a consequence of the translational invariance of the SE response of the nanowire along the longitudinal direction, the local slope is found to be independent of y_p , $\forall y_p$, $(\partial I_{\text{SE}}/\partial x)_{x_p, \text{eq}, y_p} \simeq (\partial I_{\text{SE}}/\partial x)_{x_p, \text{eq}, y_0} = G$. Each spectrum is subsequently multiplied by the local effective mass $M_{\text{eff}}(y_p)$, yielding a

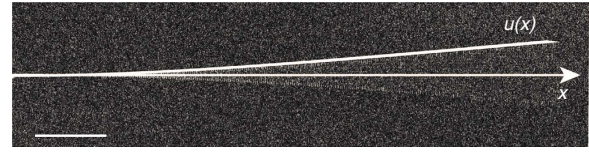


Figure 5 | Piezo-driven vibrational profile. A resonant piezo-drive is being applied to the nanowire while scanning its SE response, yielding to a stroboscopic mapping of its fundamental flexural vibrational mode (scale bar, 20 μm). The corresponding profile fits the theoretically expected mode shape given in equation 6 (straight white line), with $\beta_1 L = 1.875$ and $L = 150 \mu\text{m}$.

series of spectra $S_T[\Omega, y_p]$ (see Fig. 3b) given by:

$$S_T[\Omega, y_p] = M_{\text{eff}}(y_p) G^2 S_x[\Omega, y_p] = G^2 \times \frac{2\Gamma_{\text{eff}}(y_p) k_B T_{\text{eff}}(y_p)}{(\Omega_0^2 - \Omega^2)^2 + \Gamma_{\text{eff}}^2(y_p) \Omega^2}. \quad (5)$$

The local effective mass is independently measured from a piezo-driven vibrational profile (see Fig. 5), fitting the theoretically expected mode shape $u(x)$ (straight, white line) given by:

$$\frac{2u(x)}{u(L)} = \cosh \beta_1 x - \cos \beta_1 x + \frac{(\cos \beta_1 L + \cosh \beta_1 L)(\sin \beta_1 x - \sinh \beta_1 x)}{\sinh \beta_1 L + \sin \beta_1 L}, \quad (6)$$

with $\beta_1 L = 1.875$ and $L = 150 \mu\text{m}$.

The spectra as defined by equation (5) are integrated over the Fourier frequency, yielding in the high-Q limit ($\Gamma_{\text{eff}} \ll \Omega_0$) to a series of quantities proportional to the effective temperature:

$$\int_{-\infty}^{+\infty} \frac{d\Omega}{2\pi} S_T[\Omega, y_p] = \frac{G^2 k_B}{\Omega_M} \times T_{\text{eff}}(y_p). \quad (7)$$

Dividing equation (7) by the area of the reference spectrum $S_T[\Omega, y_0]$ subsequently yields to the cooling rate and equivalently the effective temperature $T_{\text{eff}}(y_p)$,

$$\frac{\int_{-\infty}^{+\infty} \frac{d\Omega}{2\pi} S_T[\Omega, y_p]}{\int_{-\infty}^{+\infty} \frac{d\Omega}{2\pi} S_T[\Omega, y_0]} = \frac{T_{\text{eff}}(y_p)}{T}. \quad (8)$$

References

- Cohen-Tannoudji, C. Manipulating atoms with photons. *Phys. Scr.* **1998**, 33 (1998).
- Diedrich, F., Bergquist, J., Itano, W. M. & Wineland, D. Laser cooling to the zero-point energy of motion. *Phys. Rev. Lett.* **62**, 403–406 (1989).
- O’Connell, A. D. *et al.* Quantum ground state and single-phonon control of a mechanical resonator. *Nature* **464**, 697–703 (2010).
- Anderson, M. H., Ensher, J. R., Matthews, M. R., Wieman, C. E. & Cornell, E. A. Observation of bose-einstein condensation in a dilute atomic vapor. *Science* **269**, 198–201 (1995).
- Davis, K. B. *et al.* Bose-einstein condensation in a gas of sodium atoms. *Phys. Rev. Lett.* **75**, 3969–3973 (1995).
- Inouye, S. *et al.* Observation of feshbach resonances in a bose-einstein condensate. *Nature* **392**, 151–154 (1998).
- Kielinski, D., Monroe, C. & Wineland, D. J. Architecture for a large-scale ion-trap quantum computer. *Nature* **417**, 709–711 (2002).
- Aspect, A., Dalibard, J., Heidmann, A., Salomon, C. & Cohen-Tannoudji, C. Cooling atoms with stimulated emission. *Phys. Rev. Lett.* **57**, 1688–1691 (1986).
- Raab, E., Prentiss, M., Cable, A., Chu, S. & Pritchard, D. E. Trapping of neutral sodium atoms with radiation pressure. *Phys. Rev. Lett.* **59**, 2631–2634 (1987).
- Dalibard, J. & Cohen-Tannoudji, C. Laser cooling below the doppler limit by polarization gradients: simple theoretical models. *J. Opt. Soc. Am. B* **6**, 2023–2045 (1989).
- Kasevich, M. & Chu, S. Laser cooling below a photon recoil with three-level atoms. *Phys. Rev. Lett.* **69**, 1741–1745 (1992).
- Metcalf, H. J. & Van der Straten, P. in *Laser Cooling and Trapping* (Springer, 1999).
- Arcizet, O., Cohadon, P.-F., Briant, T., Pinard, M. & Heidmann, A. Radiation-pressure cooling and optomechanical instability of a micromirror. *Nature* **444**, 71–74 (2006).
- Gigan, S. *et al.* Self-cooling of a micromirror by radiation pressure. *Nature* **444**, 67–70 (2006).

15. Schliesser, A., Riviere, R., Anetsberger, G., Arcizet, O. & Kippenberg, T. J. Resolved-sideband cooling of a micromechanical oscillator. *Nat. Phys.* **4**, 415–419 (2008).
16. Thompson, J. *et al.* Strong dispersive coupling of a high-finesse cavity to a micromechanical membrane. *Nature* **452**, 72–75 (2008).
17. Chan, J. *et al.* Laser cooling of a nanomechanical oscillator into its quantum ground state. *Nature* **478**, 89–92 (2011).
18. Teufel, J. *et al.* Sideband cooling of micromechanical motion to the quantum ground state. *Nature* **475**, 359–363 (2011).
19. Cohen-Tannoudji, C., Dupont-Roc, J. & Grynberg, G. *Atom-Photon Interactions: Basic Processes and Applications* (Wiley Online Library, 2008).
20. Kippenberg, T. J. & Vahala, K. J. Cavity optomechanics: back-action at the mesoscale. *Science* **321**, 1172–1176 (2008).
21. Wilson-Rae, I., Zoller, P. & Imamoglu, A. Laser cooling of a nanomechanical resonator mode to its quantum ground state. *Phys. Rev. Lett.* **92**, 075507 (2004).
22. Naik, A. *et al.* Cooling a nanomechanical resonator with quantum back-action. *Nature* **443**, 193–196 (2006).
23. Arcizet, O. *et al.* A single nitrogen-vacancy defect coupled to a nanomechanical oscillator. *Nat. Phys.* **7**, 879–883 (2011).
24. Rabe, J. P. & Buchholz, S. Direct observation of molecular structure and dynamics at the interface between a solid wall and an organic solution by scanning tunneling microscopy. *Phys. Rev. Lett.* **66**, 2096–2099 (1991).
25. Chan, H., Aksyuk, V., Kleiman, R., Bishop, D. & Capasso, F. Nonlinear micromechanical casimir oscillator. *Phys. Rev. Lett.* **87**, 211801 (2001).
26. Rousseau, E. *et al.* Radiative heat transfer at the nanoscale. *Nat. Photonics* **3**, 514–517 (2009).
27. Guha, B., Otey, C., Poitras, C. B., Fan, S. & Lipson, M. Near-field radiative cooling of nanostructures. *Nano Lett.* **12**, 4546–4550 (2012).
28. Garcia, R. *et al.* Identification of nanoscale dissipation processes by dynamic atomic force microscopy. *Phys. Rev. Lett.* **97**, 016103 (2006).
29. Eichler, A. *et al.* Nonlinear damping in mechanical resonators made from carbon nanotubes and graphene. *Nat. Nanotechnol.* **6**, 339–342 (2011).
30. Cole, G. D., Wilson-Rae, I., Werbach, K., Vanner, M. R. & Aspelmeyer, M. Phonon-tunnelling dissipation in mechanical resonators. *Nat. Commun.* **2**, 231 (2011).
31. Rieger, J., Isacson, A., Seitner, M. J., Kotthaus, J. P. & Weig, E. M. Energy losses of nanomechanical resonators induced by atomic force microscopy-controlled mechanical impedance mismatching. *Nat. Commun.* **5**, 3345 (2014).
32. Niguès, A., Siria, A., Vincent, P., Poncharal, P. & Bocquet, L. Ultrahigh interlayer friction in multiwalled boron nitride nanotubes. *Nat. Mater.* **13**, 688–693 (2014).
33. Nichol, J. M., Hemesath, E. R., Lauhon, L. J. & Budakian, R. Displacement detection of silicon nanowires by polarization-enhanced fiber-optic interferometry. *Appl. Phys. Lett.* **93**, 193110 (2008).
34. Glöppe, A. *et al.* Bidimensional nano-optomechanics and topological backaction in a non-conservative radiation force field. *Nat. Nanotechnol.* **9**, 920–926 (2014).
35. Baughman, R. H., Zakhidov, A. A. & de Heer, W. A. Carbon nanotubes—the route toward applications. *Science* **297**, 787–792 (2002).
36. Geim, A. K. & Novoselov, K. S. The rise of graphene. *Nat. Mater.* **6**, 183–191 (2007).
37. Goldstein, J. I. *et al.* *Scanning Electron Microscopy and X-ray Microanalysis. A Text for Biologists, Materials Scientists, and Geologists* (Plenum Publishing Corporation, 1981).
38. Buks, E. & Roukes, M. Stiction, adhesion energy, and the casimir effect in micromechanical systems. *Phys. Rev. B* **63**, 033402 (2001).
39. Seiler, H. Secondary electron emission in the scanning electron microscope. *J. Appl. Phys.* **54**, R1–R18 (1983).
40. Pinard, M., Hadjar, Y. & Heidmann, A. Effective mass in quantum effects of radiation pressure. *Eur. Phys. J. D* **7**, 107–116 (1999).
41. Cohadon, P. F., Heidmann, A. & Pinard, M. Cooling of a mirror by radiation pressure. *Phys. Rev. Lett.* **83**, 3174–3177 (1999).
42. Egerton, R., Li, P. & Malac, M. Radiation damage in the tem and sem. *Micron* **35**, 399–409 (2004).
43. Metzger, C. H. & Karrai, K. Cavity cooling of a microlever. *Nature* **432**, 1002–1005 (2004).
44. Vanlentin, L. *et al.* A comprehensive study of thermoelectric and transport properties of β -silicon carbide nanowires. *J. Appl. Phys.* **114**, 184301 (2013).
45. Wilson-Rae, I., Nooshi, N., Zwerger, W. & Kippenberg, T. Theory of ground state cooling of a mechanical oscillator using dynamical backaction. *Phys. Rev. Lett.* **99**, 093901 (2007).
46. Ikuno, T. *et al.* Thermally driven nanomechanical deflection of hybrid nanowires. *Appl. Phys. Lett.* **87**, 213104 (2005).
47. Siria, A. *et al.* X-ray pushing of a mechanical microswing. *Nanotechnology* **19**, 445501 (2008).
48. Courty, J.-M., Heidmann, A. & Pinard, M. Quantum limits of cold damping with optomechanical coupling. *Eur. Phys. J. D* **17**, 399–408 (2001).
49. Marquardt, F., Chen, J. P., Clerk, A. & Girvin, S. Quantum theory of cavity-assisted sideband cooling of mechanical motion. *Phys. Rev. Lett.* **99**, 093902 (2007).
50. Abdi, M. & Bahrampour, A. R. Improving the optomechanical entanglement and cooling by photothermal force. *Phys. Rev. A* **85**, 063839 (2012).
51. Volkert, C. A. & Minor, A. M. Focused ion beam microscopy and micromachining. *MRS Bull.* **32**, 389–399 (2007).
52. Guo, H. *et al.* Vanadium dioxide nanowire-based microthermometer for quantitative evaluation of electron beam heating. *Nat. Commun.* **5**, 4986 (2014).
53. Moser, J., Eichler, A., Güttinger, J., Dykman, M. I. & Bachtold, A. Nanotube mechanical resonators with quality factors of up to 5 million. *Nat. Nanotechnol.* **9**, 1007–1011 (2014).

Acknowledgements

Funding for this work was provided by the PSL Excellence Chair Program. A.S. acknowledges funding from the European Union's H2020 Framework Programme/ERC Starting Grant agreement no. 637748–NanoSOFT.

Author contributions

All authors contributed to all aspects of this work.

Additional information

Competing financial interests: The authors declare no competing financial interests.

Reprints and permission information is available online at <http://npg.nature.com/reprintsandpermissions/>

How to cite this article: Niguès, A. *et al.* Dynamical backaction cooling with free electrons. *Nat. Commun.* 6:8104 doi: 10.1038/ncomms9104 (2015).



This work is licensed under a Creative Commons Attribution 4.0 International License. The images or other third party material in this article are included in the article's Creative Commons license, unless indicated otherwise in the credit line; if the material is not included under the Creative Commons license, users will need to obtain permission from the license holder to reproduce the material. To view a copy of this license, visit <http://creativecommons.org/licenses/by/4.0/>